A causal link between autoantibodies and neurological symptoms in long COVID

Keyla Santos Guedes de Sa[1,2*], Julio Silva[1,2*], Rafael Bayarri-Olmos[1,2*], Ryan Brinda[1,2], Robert Alec Rath Constable[1,2], Patricia A. Colom Diaz[1,2], Dong-il Kwon[1,2,3], Gisele Rodrigues[1,2], Li Wenxue[2,4], Christopher Baker[1,2], Bornali Bhattacharjee[1,2], Jamie Wood[5], Laura Tabacof[5], Yansheng Liu[2,4], David Putrino[5†], Tamas L. Horvath[6†], Akiko Iwasaki[1,2,3†]

[1] Department of Immunobiology, Yale School of Medicine, Center for Infection and Immunity, New Haven, CT, USA
[2] Center for Infection and Immunity, Yale School of Medicine, New Haven, CT, USA.
[3] Howard Hughes Medical Institute, Chevy Chase, MD, USA
[4]Yale Cancer Biology Institute, Yale University, West Haven, CT, USA.
[5] Cohen Center for Recovery from Complex Chronic Illness, Icahn School of Medicine at Mount Sinai, New York, NY, USA
[6] Department of Neuroscience, Yale University School of Medicine, New Haven, CT 06520

* These authors contributed equally to this work as co-first authors.
[†] Correspondence: david.putrino@mountsinai.org, tamas.horvath@yale.edu, and akiko.iwasaki@yale.edu

Summary
Acute SARS-CoV-2 infection triggers the generation of diverse and functional autoantibodies (AABs), even after mild cases. Persistently elevated autoantibodies have been found in some individuals with long COVID (LC). Using a >21,000 human protein array, we identified diverse AAB targets in LC patients that correlated with their symptoms. Elevated AABs to proteins in the nervous system were found in LC patients with neurocognitive and neurological symptoms. Purified Immunoglobulin G (IgG) samples from these individuals reacted with human pons tissue and were cross-reactive with mouse sciatic nerves, spinal cord, and meninges. Antibody reactivity to sciatic nerves and meninges correlated with patient-reported headache and disorientation. Passive transfer of IgG from patients to mice led to increased sensitivity and pain, mirroring patient-reported symptoms. Similarly, mice injected with IgG showed loss of balance and coordination, reflecting donor-reported dizziness. Our findings suggest that targeting AABs could benefit some LC patients.

Keywords:
Autoantibodies, Long COVID, Chronic Pain, SARS-CoV-2

Introduction

Long COVID (LC) develops in over 10% of individuals after a SARS-CoV-2 infection[1-5]. A wide range of neurological symptoms have debilitating effects on people with LC. LC impacts multiple regions of the brain[6,7]. Women are more likely than men to develop LC and other post-acute infection syndromes (PAIS) including myalgic encephalomyelitis/chronic fatigue syndrome (ME/CFS)[8,9] affecting >1% of Americans[10,11], suggesting sex differences in the mechanisms that cause these disorders[12,13]. Since many autoimmune diseases (e.g., multiple sclerosis, rheumatoid arthritis, systemic lupus, Sjögren's syndrome) are more frequent in women, we hypothesize autoimmunity may play a central role in the development of LC and other PAIS. Although the root cause(s) of PAIS remain unclear, a wealth of data supports an autoimmune etiology of PAIS[3,14-23]. For example, AABs have been found in ME/CFS[24-26], chronic Lyme disease[27,28], and LC[3,14-23], some of which target GPCRs and GABA receptors involved in neuronal pathways relevant to neurological symptoms.

Infections naturally trigger the production of antibodies, which then clear pathogens. However, AABs often arise during infection due to bystander activation or molecular mimicry [29-34]. Diverse and functional AABs are found during the acute phase of SARS-CoV-2 infection[14,35]. Normally, AAB levels subside as the immune system returns to homeostasis [22]. However, four large independent retrospective studies of medical records from millions of patients with COVID-19 reported a 20-40% increased risk of multiple new-onset autoimmune diseases after SARS-CoV-2 infection[36-39]. Therefore, we postulate that persisting AABs may cause symptoms for some patients with LC even though these patients may not meet classical criteria to be diagnosed with known autoimmune diseases.

The heterogeneity and the current lack of understanding of the underlying mechanisms of LC pose a significant challenge in developing diagnostics and treatments. Discovering biomarkers that identify patients with AAB-driven LC would have an immediate impact, matching these patients to existing immunotherapies. Here we examined the contributions of ABB in the development of neurological symptoms afflicting LC patients. Leveraging our MY-LC cohort[40], we examined the autoreactivity of purified IgG against various human tissues and identified autoantigens using a >21,000 protein array. Importantly, we demonstrated that passive transfer of these purified IgG samples to healthy C57BL/6 mice recapitulated phenotypes of neurological symptoms in the donors.

Methods

Ethics statement involving human studies

This study was approved by the Mount Sinai Program for the Protection of Human Subjects (IRB 20-01758) and Yale Institutional Review Board (IRB 2000029451 for MY-LC; IRB 2000028924 for enrolment of pre-vaccinated Healthy Controls). Informed consent was obtained from all enrolled participants.

MY-LC enrollment

MY-LC study design, inclusion, and exclusion criteria for recruitment of individuals have been described in detail, previously[40,41]. Briefly, individuals experiencing persistent symptoms for > 6 weeks after initial SARS-CoV-2 infection were invited to participate in the study from various LC clinics within the Mount Sinai Health System and the Cohen Center for Recovery from Complex Chronic Illness at The Mount Sinai Hospital. The participants who enrolled in the LC group underwent complete medical evaluations by physicians to rule out alternative medical etiologies for their persistent symptoms before study enrolment. Those joining either the healthy or convalescent study groups were recruited through IRB-approved advertisements disseminated via email lists, study flyers in hospital public areas, and various social media platforms. Before enrollment, all participants provided informed consent. On the day of sample collection, each participant supplied peripheral blood samples and completed symptom surveys. Additionally, self-reported medical histories of all participants in the MY-LC cohort were collected during study visits and cross-checked by collaborating clinicians through the examination of electronic medical records.

Purification of immunoglobulins

Total IgG was purified from serum samples using Protein-G beads (Sigma-Aldrich, St. Louis, MO, US). One and a half mL of serum samples were diluted 1:2 with phosphate-buffered saline (PBS) and incubated with 2 mL of Protein-G Sepharose beads (Millipore Sigma, GE17-0618-05) overnight (ON) at 4 °C. Samples were transferred to elution columns and depleted sera (flow-through) was collected and stored at –80°C for later use. Beads were washed 3 times with PBS, and eluted using 100 mM glycine pH 2.3 into six fractions. The eluates were neutralized to pH 7.4 using 1 M Tris pH 8, centrifuged, and the protein concentration was determined using a NanoDrop 8000 (Thermo Fisher Scientific, Waltham, MA, US). Fractions containing antibodies were pooled and dialyzed ON in PBS at 4°C. Dialyzed samples were quantified, aliquoted, and stored at 4°C.

Characterization of human IgG purity and homogeneity

Fast Protein Liquid Chromatography (FPLC) was performed using a Quest 10 Plus NGC Chromatography System (Bio-Rad Laboratories Inc., Hercules, CA, US; 7880003) fitted with an ENrich SEC 650 10x300 column (Bio-Rad, 780-1650) equilibrated with filtered and degassed PBS. Fifty µL of total human IgG at 1 mg/mL (total 0.05 mg) were injected into the column at a flow rate of 0.5 mL/min. Bovine thyroglobulin (670 kDa), bovine γ-globulin (158 kDa), and chicken ovalbumin (44 kDa) (all from the gel filtration standard, Bio-Rad, 1511901)

were used to estimate the MW of the IgG elution peaks. The SEC traces were analyzed using ChromLab Software (Bio-Rad).

Autoantigen pull down

At 6-8 weeks of age, four female C57BL/6J mice were euthanized with isoflurane and perfused with PBS. The whole brain was dissected, and placed into 1 mL of non-denaturing lysis buffer (20 mM Tris HCl pH 8, 137 mM NaCl, 1% Nonidet P-40, 2 mM EDTA) with complete protease inhibitor cocktail (Roche, Sigma, 11697498001) on ice. Tissues were then homogenized with MP FastPrep -24 at speed 2 for 20 s, then centrifuged at 14,000 g for 10 min, at 4 °C. The supernatant was aliquoted and frozen at −20 °C until use. For pre-clearing of supernatants, Protein G Sepharose beads (Millipore Sigma, GE17-0618-05) were washed with non-denaturing lysis buffer with complete protease inhibitor cocktail, then equilibrated in PBS. Subsequently, 100 µL beads were incubated with 100 µL pooled brain supernatant, constantly mixing for 1 h, at 4 °C. Beads were pelleted at 100 g for 3 min at 4 °C, discarded and the supernatant extracted.

Four µg of total IgG purified from the participants were mixed with Protein G Sepharose beads (Millipore Sigma, GE17-0618-05) and incubated ON at 4 °C in a rocking platform. IgG/protein G bead complexes were incubated with pre-cleared supernatants ON at 4 °C in a rocking platform. Beads were recovered by centrifugation at 100 g for 3 min at 4 °C, then washed 4 times with non-denaturing lysis buffer with complete protease inhibitor cocktail. Beads were again recovered by centrifugation, then eluted using 100 µL of elution buffer (100 mM glycine pH 2.3). The eluates were neutralized to pH 7.4 using 1 M Tris pH 8, centrifuged, and dialyzed ON in PBS at 4 °C. Dialyzed samples were quantified by NanoDrop 8000 (Thermo Fisher Scientific, Waltham, MA, US), aliquoted, and stored at 4 °C.

Mass spectrometry sample preparation and data procession

A total 20 µL of above immunoprecipitated samples were digested for the mass spectrometry-based proteomic analysis. For each sample, 30 µL of 10 M urea was added. Reduction and alkylation were carried out using 10 mM Dithiothreitol (DTT) for 1 hour at 56°C, followed by 20 mM iodoacetamide (IAA) in darkness for 45 minutes at room temperature. The samples were then diluted with 100 mM NH4HCO3 and digested with trypsin (Promega) at a ratio of 1:20 (w/w) overnight at 37°C. The purification of the digested peptides was performed using a C18 column (MacroSpin Columns, NEST Group INC). About 1 µg of the peptide was injected for mass spectrometry measurement.

The samples were measured by a data-independent acquisition (DIA) MS method as described previously [42,43], on an Orbitrap Fusion Tribrid mass spectrometer (Thermo Scientific) coupled to a nanoelectrospray ion source (NanoFlex, Thermo Scientific) and an EASY-nLC 1200 system (Thermo Scientific, San Jose, CA). A 120-min gradient was used for the data acquisition at the flow rate at 300 nL/min with the column temperature controlled at 60 °C using a column oven (PRSO-V1, Sonation GmbH, Biberach, Germany). The DIA-MS method consisted of one MS1 scan and 33 MS2 scans of variable isolated windows with 1 m/z overlapping between windows. The MS1 scan range was 350 – 1650 m/z and the MS1 resolution was 120,000 at m/z 200. The MS1 full scan AGC target value was set to be 2E6 and the maximum injection time was 100 ms. The MS2 resolution was set to 30,000 at m/z 200 with the MS2 scan range 200 – 1800 m/z and

the normalized HCD collision energy was 28%. The MS2 AGC was set to be 1.5E6 and the maximum injection time was 50 ms. The default peptide charge state was set to 2. Both MS1 and MS2 spectra were recorded in profile mode. DIA-MS data analysis was performed using Spectronaut v18[44] with directDIA algorithm by searching against the SwissProt mouse fasta sequences (September 2022). The oxidation at methionine was set as variable modification, whereas carbamidomethylation at cysteine was set as fixed modification. Both peptide and protein FDR cutoffs (Qvalue) were controlled below 1% and the resulting quantitative data matrix were exported from Spectronaut. The sample normalization was off. All the other settings in Spectronaut were kept as Default.

Immunofluorescence staining

Mice were anesthetized and perfused with PBS and 4% paraformaldehyde (PFA). For meninges analyses, NG2DsRedBAC (Jackson, 008241) was used. Target tissues were harvested and postfixed ON with 4% PFA, embedded in optimal cutting temperature (OCT) compound (Sakura Finetek, Torrance, CA, US) and then frozen on a cooling bath with acetone/dry ice. Tissues were stored at –80 °C. Tissues were sectioned with a cryostat at a thickness of 10 µm and thaw mounted onto SuperFrost Plus Slides (Thermo Fisher Scientific). Slides were stored at – 80 °C until use.

Slides were thawed at room temperature (RT) and washed in PBS to remove excess OCT. Samples were outlined using a hydrophobic PAP pen. Slides were blocked with a solution of 1% bovine serum albumin (BSA) and glycine (22 mg/mL) in a humidified chamber for 1 h. A 0.3% Sudan Black B/70% ethyl alcohol (EtOH) solution was added to each sample and incubated before being washed thoroughly with PBS. Samples were incubated with 0.039 mg/ml of purified total IgG. For stain endothelial cells in the meninges, the samples were also incubated with Alexa Fluor® 647 anti-mouse CD31 Antibody (Biolegend, 102516). Each sample was assigned a patient antibody ID number and incubated with said patient IgG in a humidified chamber ON. Slides were washed in PBS and incubated with Alexa Fluor® 488 AffiniPure™ Donkey Anti-Human IgG (Jackson ImmunoResearch, 709-545-149) in a humidified chamber for 60 min, for Human-on-Human immunofluorescence the total IgG purified from the patients were labeled with Alexa Fluor 488 using Alexa Fluor 488 Protein Labeling Kit (Themo Fisher Scientific, A10235), without the use of secondary antibody. Slides were once again washed in PBS and immersed in distilled water. Washed slides were mounted with a solution of DAPI Prolong® Gold antifade reagent (Invitrogen, Thermo Fisher Scientific, P36930) with 17.5 µg/ml of DAPI and covered with a coverslip. Slides were stored in the dark at 4 °C. Images were acquired by the Stellaris Confocal microscope at ×20 magnification and LAS X software (both from Leica Microsystems, Wetzlar, Germany). The percentage of stained area and mean of fluorescence were calculated using ImageJ software.

Autoantibody analysis by HuProt

Plasma samples were analyzed using the ImmuneProfiler on HuProt™ human proteome arrays (CDI Laboratories, Baltimore, MD, US). Arrays and plasma samples, diluted 1:1000 into CDISampleBuffer, were blocked for 1 h. Each blocked and diluted sample was then probed onto a HuProt™ microarray for 1 h. Following the probing step, the arrays underwent three 10-min washes with TBS-T (TBS, 0.1% Tween 20). Subsequently, they were probed with Alexa 647-anti-human IgG Fc specific for 1 h within a light-proof box. This was followed by three washes

with TBS-T, each lasting 10 min, and three rinses with ddH_2O. Blocking and all incubation steps were performed at RT with gentle shaking. The arrays were then dried with an air duster and scanned using a GenePix® 4000B scanner (Molecular Devices, San Jose, CA, US).

Validation of autoantigens by ELISA

Top hits identified by HuProt™, MED20 (MyBiosource, San Diego, CA, US; MBS5308819) and USP5 (MyBiosource, MBS8121224), were coated on Maxisorb microtiter 96-well plates (Thermo Fisher Scientific, 439454) in a 2-fold dilution (starting concentration 10 µg/ml) ON at 4 °C. Plates were washed three times using PBS-T (PBS, 0.05% Tween 20), and the buffer was left in the wells for 1 h before applying the samples Purified human IgG at a concentration of 25 µg/mL and 10 µg/mL in PBS-T with 2% fetal calf serum was added to the plates and incubated for 2 h at RT shaking at 80 rpm. Plates were washed three times using PBS-T and incubated with polyclonal rabbit anti-human IgG/HRP (1:2,000; Agilent P021402-2) for 1 h at RT shaking at 80 rpm. Plates were washed five times using PBS-T and incubated in the dark with 100 µl/well of 1-Step Ultra TMB (Thermo Fisher Scientific, 34029) for 10 min. The reaction was stopped with 50 µl of 0.5 M H_2SO_4. The plates were read at 450 nm with 630 nm subtraction on a Cytation 5 reader (BioTek).

Animals

Behavioral experiments were performed on C57BL/6J (Jackson Laboratory, stock number 000664) female mice aged between six and eight weeks. Mice were maintained under specific pathogen-free conditions at Yale University. Mice were maintained in ventilated cages at an ambient temperature and humidity-controlled room with a 12 h light/12 h dark cycle with continuous access to food and water. The experiments using animals were performed according to the federal guidelines and the institutional policies of the Yale School of Medicine Animal Care and Use Committee (Approved Protocol 2021-10365).

Passive transfer and behavior analysis

Mice were injected intraperitoneally with 38 mg/kg of total IgG from participants (Healthy Controls, Convalescent Controls and LC) or with PBS. Mice were co-housed with each cage having one mouse per condition. All the experiments were performed between 1-6 pm and mice were allowed to acclimate in the room for at least 1 h.

Open Field Test

The Open Field test was performed to characterize locomotor activity and anxiety-like behaviors. The apparatus consisted of a 50 cm × 50 cm arena surrounded by 45 cm opaque plexiglass walls. For testing, the mice were placed in the center of the arena, and left to explore for 10 min, after which they were returned to their home cage. EthoVision XT 15 software (Noldus, Wageningen, the Netherlands) was used to track distance traveled in central and peripheral zones, the ratio of time spent in central and peripheral zones, movement, distance traveled, activity and velocity.

Elevated Zero Maze Test

Elevated Zero Maze was administered to measure anxiety-like behaviors and behavioral disinhibition. The apparatus consisted of an O-ring arena elevated 60 cm above the ground, with two opposing arms enclosed in plexiglass walls (50 cm × 10 cm × 40 cm) and

two opposing open arms (50 cm × 10 cm). Mice were placed in the open arm, and left to explore the arena for 5 min, after which they were returned to their home cage. EthoVision XT 15 software was used to track movement, velocity, and time spent in the closed and open arms.

Rotarod

To assess the motor coordination of the mice, an accelerated rotarod test was performed. On test day, mice were placed on the resting rotarod apparatus (Ugo Basile, Gemonio, Italy) for at least 1 min. The speed of the rotarod was accelerated from 4 to 80 rpm over a 300 s period. The mice were subjected to four trials with at least 15 min intervals between trials. The retention time of the rod in each trial was recorded and the average of all the trials was plotted.

Grip Strength Test

Limb strength (fore and hind limb) was assessed using a commercially available grip strength meter (Ugo Basile), incorporating a stainless-steel orientable grid and force transducer. The mice were held gently by the base of the tail and pulled across the horizontal orientable grid so that they were able to grip the bar with their four paws. A digital readout of the maximum force applied is given once the grip is released. The test was performed at least three times on each mouse to measure force values.

Hot Plate test

To evaluate thermal sensitivity, mice were placed on a hot plate (Ugo Basile) with the plate set at 55°C. The time to the first sign of nociception (i.e. paw licking, flinching, or jump response) was measured and the animal was immediately removed from the hot plate. A cut-off period of 20 s was maintained to avoid damage to the paws.

Blood Pressure and Heart Rate

Measurement of mouse blood pressure was carried out using the CODA mouse tail-cuff blood pressure system (Kent Scientific Corp., Torrington, CT, US). Measurements were made during the afternoon (1-6 pm) with the mice awake, restrained on CODA apparatus and lying down on a warm plate, covered with a dark blanket. Each blood pressure measurement was carried out for 20 cycles for acclimatation and 20 cycles with recording with a deflation time of 20 s. The mean blood pressure, systolic blood pressure, diastolic blood pressure and heart rate were determined by the average of all 20 measurements during the recording cycles.

Statistical analysis

For immunofluorescence analyses, the threshold for positivity was defined as the mean fluorescence of healthy control staining plus two times the standard deviation and represented as a dashed line. The threshold of positivity of plasma auto-reactivities in the HuProt™ array was determined as three times the mean of controls.

To classify the mice that were positive or negative to a specific symptom, the threshold was defined as the mean of the healthy control group plus one time the standard deviation and represented as a dashed line.

Multiple group comparisons were performed with one-way analysis of variance (ANOVA) followed by Tukey's multiple comparisons correction. The differences in the values obtained for two different groups were evaluated using an unpaired, two-tailed Student's t test

with 95% confidence interval. The differences in the frequency of participants or mice that were positive for a specific symptom were evaluated by Chi-square test. Analyses were performed using the GraphPad PRISM (Version 10.2.3; GraphPad, San Diego, CA, US).

Results

IgG targeting the CNS and PNS correlate with neurological symptoms in LC

From our Mount Sinai-Yale LC (MY-LC) cohort [40], we identified and focused on a subset of LC participants with high neurological symptom burden (n=55). This group was predominantly comprised of women (**Figure 1A**) with an average age of 46.3 years (**Figure 1B**), with no statistical differences between genders when compared to the convalescent controls (n = 42, CC) or healthy controls (n = 39, HC). These patients exhibited neurological symptoms, with 63.6% of them experiencing five or more, and 52.7% experiencing mild LC disease (defined by LC propensity score [LCPS] using a parsimonious logistic regression model as described[40]) (**Figure 1C**). The most common neurological symptoms were brain fog (80.0%), headache (65.4%), loss of memory (64.4%), dizziness (58.2%), sleeping disturbance (58.2%), and confusion (54.5%). At the time of enrollment, these individuals reported not having an autoimmune diagnosis.

To evaluate if study participants had functional AAB profiles that could provoke their LC-associated neurological symptoms, we purified total IgG from plasma and performed immunofluorescence analyses using healthy human tissues (**Figure 1D**). To determine if patients' IgG cross-react to mouse tissues, we also included a large collection of mouse tissues for staining (**Figure 1D**). We observed that purified total IgG from LC participants showed increased reactivity against human pons (**Figure 1E**), mouse sciatic nerve (**Figure 1F**), mouse meninges (**Figure 1G**), and mouse cerebellum (**Figure 1H**). Few participants also displayed positivity against mouse spinal cord (**Supp. 1A**), thalamus and hypothalamus, hindbrain, cerebral nuclei, cerebral cortex, and hippocampus (**Supp. 1B**), but not against non-neural tissues (**Supp. 1C**). Thus, IgG from patients with LC are selectively cross-reactive to neural tissues.

Next, we analyzed whether cross-reactive antibodies to CNS correlate with the donors' LC symptoms. The mean of fluorescence and positive staining by patients' IgG for mouse meninges was associated with headache, and with an enrichment of the positive staining in loss of memory, weakness, and disorientation (**Figure 2A**). None of the other symptoms evaluated were significantly associated with meninges stain (**Supp 2A**). To evaluate the specificity of the AAB recognition of the meninges, tissue was co-stained using antibodies to NG2-dsRED (a marker for pericyte) and CD31 (endothelial cell marker). We observed that the staining with IgG from LC participants mostly co-localized with pericytes and somewhat with endothelial cells and radiated out to the surrounding tissues beyond the pericytes (**Figure 2B**).

We observed that LC patients with tinnitus have increased mean fluorescence staining for the sciatic nerve, albeit not significant (**Figure 2C**). None of the other symptoms evaluated were significantly associated with sciatic nerve stains (**Supp 2B**).

We also observed significant diversity in the stains, with different participants showing positive stains for different tissues and exhibiting distinct stains patterns (**Figure 2D**). Notably, IgG from a subset of patients exhibited a wide range of cross-reactivities against the majority of the neurological tissues examined.

Identification of autoantibody targets

To identify AAB targets, we screened patient plasma using the HuProt™ microarray containing >21,000 human proteins (**Figure 3A**). Using a negative binomial (NB) regression

with longlink function of positive auto-reactivities (i.e. >3 times the mean on controls), we observed that LC participants had an increased number of autoreactive antibodies compared to controls (**Figure 3B**). Similar to the increase in staining patterns observed with the immunofluorescence analysis, LC participants had a significant increase in the diversity of positive hits (**Figure 3C**), with many targeting CNS antigens (**Figure 3D, E**). We performed an unsupervised clustering based on all the 21,000 full-length proteins evaluated with the HuProt™ array and found a cluster enriched in LC patients, showing increased autoreactivities to neurological proteins (**Figure 3F**). IgG from patients with LC also showed increased reactivity to common autoantigens (**Figure 3G**).

To confirm the array results, we performed an unbiased autoantigen screening by pulling down antigens from precleared brain extracts using Protein G beads loaded with total IgG purified from four healthy controls and four LC, followed by mass spectrometry analysis. IgG purity and homogeneity were confirmed by size-exclusion chromatography (**Supp. Fig. Fig. 3A**). We identified peptides belonging to the same protein family as the top HuProt™ hits, USP5 and MED20. Moreover, the top hits targets identified by HuProt and MS were further validated by ELISA. The participants identified by HuProt as positive for MED20 and USP5 showed IgG reactivity by ELISA using serial dilutions of the autoantigens and two different concentrations of AAB (25 µg/mL **Figure 3H-I**, and 10 µg/mL **Supp. Fig. 3C**).

Transfer of IgG from patients with LC into mice recapitulates pain, loss of balance and coordination, and muscle weakness

To evaluate if AABs identified in the LC participants are pathogenic, we developed a mouse passive transfer model. Mice received 38 mg/kg of total IgG intraperitoneally (IP), with each mouse receiving IgG from a different donor. The mice were co-housed, with each cage housing one mouse that received an injection of PBS, IgG from Healthy Control, Convalescent Control, or LC donors. All the behavioral experiments were performed between 1-6pm (**Figure 4A**).

After the injection we evaluated the presence of hIgG in the brain and serum. At 24 h post-injection, we observed hIgG crossing the BBB and the concentration of antibodies remained relatively constant for five days (**Supp. Fig. 3D**). Five days after injection, we observed that 5% of the human IgG crossed the blood-brain barrier, as measured by ELISA of brain homogenates, (**Figure 4B**), and that at day three post-injection these mice displayed increased thermal pain sensitivity based on the hot plate test (**Figure 4C**). When we compared the hot plate test with the symptoms that the donors displayed, we observed that mice receiving IgG from those diagnosed with chronic pain (inflammatory pain or neuropathic pain) displayed enhanced pain sensitivity at the hot plate test (**Figure 4D**), with 85% of the mice with the pain phenotype (i.e. defined by the threshold for pain positivity) having received IgG from participants with LC who self-reported new-onset pain since their LC diagnosis (**Figure 4E**). The hot plate test was also associated with pain sensations described by the LC participants as pins and needles and burning pain, and a non-statistically significant trend with electric shock (**Figure 4F-H**). The hot plate test phenotype was also associated with weakness and dysautonomia, with 55% of the mice scoring positive for pain receiving IgG from patients who reported weakness and 90% from patients with dysautonomia (**Figure 4I-J**). All the other symptoms evaluated were not significantly associated with the hot plate test (**Supp. Fig. 4A**).

The grip strength test (carried out on day three post-injection) showed a trend of muscle weakness in mice injected with IgG from those with LC (**Figure 4K**). When we segregated by symptoms, we observed an association with tinnitus (54.5% of the mice that showed muscle weakness received IgG from participants who had tinnitus) (**Figure 4L**). We also observed a trend when we compared the grip strength test with the participants who reported headaches (90.9% of the mice with muscle weakness were injected with IgG from participants reporting headaches) (**Figure 4M**). All the other symptoms evaluated were not significant (**Supp. Fig. 4B**).

The rotarod test was evaluated two days post-injection. While we did not observe significant differences when comparing across the groups (**Figure 4N**), when we evaluated symptoms reported by LC participants, we observed that 88.88% of the mice that showed loss of balance and coordination had received IgG from patients who reported dizziness (**Figure 4O**). All the other symptoms evaluated were not significant (**Supp. Fig. 5A**). These observations are consistent with the positive IgG staining for the spinal cord, meninges, cerebellum, and sciatic nerve (**Figure 1**; **Supp. Fig. 1**).

To evaluate how those antibodies may be inducing pain, we performed the passive transfer using a Scn10a-Cre::tdTomato mice, with fluorescent labeling of sodium channel Na(v)1.8 specifically expressed in dorsal root ganglion (DRG) and peripheral nerve axons that mediates pain [45]. We observed that mice injected with IgG from patients with LC had a reduction in the number and volume of Intraepidermal Nerves Fibers (IENF) when compared with mice that received IgG from healthy controls (**Figure 4P**). The reduction in the IENF is a marker for Small Fiber Neuropathy (SFN) [46] that usually presents with chronic pain described as burning pain and/or pins and needles sensations (both symptoms were associated with the hot plate test results) (**Figure 4F-G**). We also evaluated anxiety-like behavior and locomotion by open field and elevated zero maze (**Supp. Fig. 6A-C**), and blood pressure and heart rate (**Supp. Fig. 6D**) to evaluate pathological changes to orthostatic responses. We did not observe significant differences in these tests between the groups receiving IgG from HC, CC, or LC participants.

Together these data show that passive total IgG transfer from people with LC induces heightened pain sensitivity, loss of balance and coordination, and muscle weakness in mice, and is associated with the symptoms reported by those participants, namely chronic pain, headache, tinnitus, dizziness and dysautonomia.

Discussion

In this study, we evaluated the presence of AABs and their pathological potential in LC. Our data show that a subset of LC participants had AAB against human pons, and cross-reactive antibodies against mouse tissues, mostly focused on neurological tissues. By employing a comprehensive human autoantigen microarray, we demonstrated that LC patients' IgG react against a wide array of antigens that are enriched in the nervous system tissues. We validated some of the microarray hits using two other orthogonal methods, MS and ELISA. To evaluate their pathogenic potential, we passively transferred purified IgG from patients into mice and showed that these antibodies are sufficient to recapitulate key neurological symptoms described by the patients with LC. Collectively, our data illustrate the pivotal role of autoantibodies as a key driver of neurological disorders in LC and suggest their utility in the diagnosis of this LC endotype.

Using a broad range of tissues and performing immunofluorescence using total IgG purified from LC participants, we were able to identify a subset of participants with AAB against neurological tissues and symptoms that are more closely associated with those AAB. A recent case report[18] also showed cross-reactive antibodies in the cerebrospinal fluid against several mouse neurological tissues, including meninges and sciatic nerve in a patient with severe neurological symptoms following SARS-CoV-2 infection.

Among participants with cross-reactive antibodies against mouse meninges, we observed co-localization of those antibodies with pericytes. AAB against pericytes may explain its association with reported headache by LC participants, since changes in pericyte functions have been described to play a role in the vascular mechanisms associated with migraine with aura[47]. LC participants with reported tinnitus had increased cross-reactive antibodies against mouse sciatic nerve. Despite being considered rare, peripheral neuropathy has been associated with tinnitus[48,49], also described as Auditory Neuropathy Spectrum (ANS), and may be explained by cochlear neural degeneration even in participants with normal hearing [50].

One important aspect of our findings is the high diversity of AAB found in those participants, illustrated by the staining patterns and the HuProt™ data. This diversity is expected since LC likely consists of multiple endotypes, with a broad range of symptoms that vary from person to person, with distinct disease drivers including persistent virus, herpesvirus reactivation, tissue damage, and autoimmunity [51]. In our cohort, we observed that chronic pain is the symptom most strongly associated with AABs, followed by other symptoms, such as headache, tinnitus, and dizziness.

Using a human protein array, mass spectrometry and ELISA, we identified and validated MED20 and USP5 as top targets for AAB. AABs against these proteins may play a role in the development of LC neurological symptoms since Mediator Complex (MED) proteins, such as MED12 and MED23 have been associated with neurological diseases [52,53]. In addition, USP5 has been associated with chronic pain[54] due to its functions as a deubiquitinase that specifically removes the ubiquitination modification from Cav3.2 channels, a T-type calcium channel that regulates the excitability of nociceptive neurons, increasing their stability and stimulating [54]. Knockdown of USP5 has been shown to induce analgesia [54] It should be noted that reactivity against MED20 or USP5 was present in only a subset of LC patients, emphasizing the diversity of AABs and LC phenotypes.

For the LC endotype driven by AABs, there may be existing therapies that would counter the pathologic impacts of the AABs. For example, intravenous immunoglobulin (IVIg)

treatment might work by neutralization and clearance of AABs [55]. An analysis of 130 cases including IVIg treatment for neuro-COVID reveals that this technique is beneficial for patients with LC and ME/CFS[56]. A review of IVIg usage in post-COVID neurological disorders revealed that while virtually all studies showed benefit from IVIg treatment in patients with post-COVID neurological disorders, only 12 of 76 case reports (16%) demonstrated unequivocal diagnoses of autoimmune encephalitis, and one in every four of these cases (26%) lacked evidence to support such a diagnosis[56]. Benefits from IVIg treatment was also reported in LC patients with small fiber neuropathy[57]. However, IVIg does not help all patients, and currently there are no guidelines or clinical tests to distinguish between those who would benefit and those who do not, underscoring the urgent need to develop new biomarkers. Demonstration of functional AAB may be used as a diagnostic tool to inform IVIg therapy. In addition to IVIg, AAB-driven disease may be treatable with mechanisms to degrade circulating antibodies (e.g., FcRn inhibitors), neutralize their action (e.g., BC 007), or remove them temporarily (e.g., plasmapheresis), or targeting of antibody-secreting cells (e.g., anti-CD20 monoclonal antibodies or CAR-T) may be considered.

Limitations of our study include the lack of identification of autoantigens sufficient to mediate the pathological phenotype, and the effector functions utilized by the AAB to mediate tissue damage. Although our experimental approach does not address directly the mechanisms by which AAB induce the symptoms reported by LC participants, the findings described here will enable future studies to identify the autoantigens that trigger pathology in mice and characterize the effector function of those AAB. Furthermore, determining which AAB targets cause LC will open the door to the development of novel treatments, such as next-generation target-specific immunotherapies.

Currently, AABs are not widely recognized as a driver of post-COVID neurological symptoms. Based on our data, an array of common autoantigens or a broad array of comprehensive human proteome would not be suitable as a tool to diagnose AAB-LC endotype. Effective diagnosis of this LC endotype will likely require an optimized panel of autoantigens that can sensitively and accurately detect functional AABs. In the absence of such tools, passive transfer of IgG from patients into mice followed by measurement of key validated behavioral phenotypes could provide an interim method, although not scalable. Finally, the use of blood products including immunoglobulins from people with LC in treatment settings requires careful consideration, as they may pose pathologic risks to the recipients. Our data provide key pathological roles of AAB in driving neurological phenotypes in vivo and warrant future studies to inform diagnosis and therapy for this subset of LC.

Acknowledgements

We thank the members of community of MY-LC study participants who volunteered both their time and effort in aiding the completion of this study, and who also helped to inform and educate on the effective and equitable communication of the results from this study.
We are also grateful to Huiping Dong, Melissa Linehan, Suzanne Fischer and Pavlina Baevova for technical support.
Various graphical schematics were created using BioRender.
We thank Nils Kort for providing the meninges from NG2-dsRed mice.
This work was supported by the Else Kröner Fresenius Prize for Medical Research 2023, grants from the National Institute of Allergy and Infectious Diseases (R01AI157488 to A.I.), RTW Foundation (D.P.), the Howard Hughes Medical Institute Collaborative COVID-19 Initiative (A.I.), Howard Hughes Medical Institute Emerging Pathogens Initiative (A.I.), and the Howard Hughes Medical Institute (A.I.). Steve and Alexandra Cohen Foundation (D.P. and J.W.), Nash Family Foundation (D.P. and J.W.) and Polybio Research Foundation (D.P. and J.W.). K.S.G.S. receive research support from Pew Latin American Fellowship.

Author contributions

K.S.G.S., J.S. and R.B.O designed and performed the experiments, analyzed the data, generated the figures, and wrote the manuscript. R.B., R.C., P.C.D., D.K., G.R., L.W. and C.B. performed experiments and helped with data interpretation. B.B, J.W., L.T., Y.L., D.P., T.L.H. and A.I. provided reagents, helped with data interpretation, discussed the hypotheses, and assisted in manuscript revisions. A.I. supervised the project, designed the experiments, helped with data interpretation, participated in the data analysis, and wrote the manuscript.

Declaration of interests

A. I. co-founded RIGImmune, Xanadu Bio and PanV and is a member of the Board of Directors of Roche Holding Ltd and Genentech. All other authors declare no competing interests.

Figure Legends

Figure 1. Purified IgG from participants with Long COVID reacts with CNS and PNS tissues. A-C. Demographics (gender, age and symptoms) of biospecimens analyzed from MY-LC cohort. **D-H.** Confocal microscopy showing human and mouse tissues immunostained with human total IgG (green) purified from Long COVID, healthy or convalescent controls, as indicated, and nuclear DNA stain (DAPI, blue). **D.** Experiment schematic. **C.** Representative images of human pons immunostaining and Mean of fluorescence intensity. **F.** Representative images of mouse sciatic nerve immunostaining and mean of fluorescence. **G.** Representative images of mouse meninges immunostaining and mean of fluorescence. **H.** Representative images of mouse meninges immunostaining and mean of fluorescence. Scale bar described in the image. Insets indicate a higher magnification of a region indicated (red rectangle). Each dot in the figure represents the value obtained from an individual participant. Data are presented as the mean. Significant p-values are described in the image, as determined by One-way ANOVA with Tukey multiple comparisons test.

Figure 2. IgG from participants with long COVID that reacts to meninges and sciatic nerve are associated with symptoms. A. Mouse meninges stain divided by symptoms displayed by the participants, as headache, memory, weakness and disorientation. **B.** Confocal microscopy showing meninge from NG2-dsRED mouse stained with total IgG from Long COVID participant (green) and CD31 (yellow), NG2-dsRED stains in red, nuclear DNA stain in blue (Dapi). Line scan analysis showing fluorescent intensity for hIgG, CD31 and NG2-dsRED. White line indicates the scan analysis in the graph. Scale bar described in the image. **C.** Mouse sciatic nerve stain divided by symptoms displayed by the participants, as tinnitus. **D.** Heatmap showing positive stain pattern across different tissues between participants, each collum is a different participant, each row is a different tissue. Each dot in the figure represents the value obtained from an individual participant. Data are presented as the mean. Significant p-values are described in the image, as determined by One-way ANOVA with Tukey multiple comparisons test.

Figure 3. Individuals with Long COVID demonstrate elevated autoantibody reactivity including to CNS tissues. A. Plasma from participants were incubated with HuProt microarray and probed with a secondary antibody against human IgG, positive targets were identified using an microarray scanner. **B.** Number of HuProt-derived auto-reactivities for each person within each group starting at a HuProt intensity threshold of >3x the mean of controls. Model was run using negative binomial (NB) regression with longlink function. Dispersion-adjusted incidence rate ratio for each group was compared to the overall mean using analysis of Means (ANOM), with significance adjustment using the Nelson method. Each point denotes the count of HuProt positive hits for an individual. **C.** Heatmap depicting the incidence rate ratios derived from negative binomial regression for each group at HuProt thresholds between 2-3x the signal intensity of the control mean, as in A. Asterisks denote significance from the adjusted overall mean using NB-derived ANOM with significance adjustment using the Nelson method. **D.** Heatmap depicting HuProt autoantibody reactivity to CNS starting at HuProt scores of >=3x. Each column represents a single participant and each row represents a single protein. **E.** Heatmap depicting the incidence rate ratio difference between each respective group and the mean of all groups using Poisson Regression with ANOM analysis followed by Nelson correction. Asterisks

denote significance. **F.** Heatmap showing unsupervised cluster analysis for HuProt autoantibody reactivity. **G.** Heatmap depicting HuProt autoantibody reactivity to common antigens by group starting at HuProt scores of >=2.8x. **H-I.** ELISA and Area Uder Curve (AUC) analysis for top hit targets identified by Huprot.

Figure 4. **IgG from individuals with LC induces symptoms in mice. A** A dose of 38 mg/kg of total IgG purified from healthy, convalescent controls and Long COVID participants were administered to 6-8 weeks-old C57BL/6 female mice by intraperitoneal (IP) injection, which were followed up for 5 days. **B** Quantification of human IgG by ELISA in brain homogenate and serum at day 5 post-injection. **C** Hot plate test performed on day 3 post injection. **D** Hot plate test divided by status of chronic pain displayed by the participants. **E** Frequency of mice with pain at the hot plate test and the patients with diagnosed chronic pain. **F-H** Hot plate test divided by how the participants described their pain sensation. **I** Hot plate test divided by participants that displayed weakness. **J** Hot plate test divided by participants that displayed dysautonomia. **K** Grip strength test performed on day 3 post injection. **L** Grip strength test divided by participants that displayed tinnitus. **M** Grip strength test divided by participants that displayed headache. **N** Rotarod test performed on day 2 post injection. **O** Rotarod test divided by participants that displayed dizziness. **P** Longitudinal Two-photon imaging of Scn10a-Cre::td Tomato reporter mice reveals collagen fibers by second harmonic generation (SHG) as well as nociceptor axons and the perpendicular intraepidermal nerve fibers (IENF; white/pink). Quantification of total IENF volume and number of fibers crossing the dermis boundary after passive transfer. Scale bars 50μm. Each dot in the figure represents the value obtained from an individual mouse. Each mouse received antibodies isolated from a single human participant. Data are presented as the mean. Significant p values are described in the image, as determined by T-test for two groups comparison or one-way ANOVA corrected for multiple comparisons with Tukey test for multiple groups comparison.

Supplemental Information

Supplementary Figure 1. AAB from a small subset of Long COVID participants are restricted to with CNS and PNS tissues. Confocal microscopy showing human and mouse tissues immunostained with human total IgG (green) purified from Long COVID, healthy or convalescent controls, as indicated, and nuclear DNA stain (DAPI, blue). **A** Representative images of mouse spinal cord immunostaining and mean of fluorescence intensity. **B** Mean of fluorescence for mouse thalamus plus hypothalamus, hindbrain, cerebral nuclei, cerebral cortex, hippocampus, anterior olfactory nucleous and midbrain. **C** Mean of fluorescence for human adrenal gland, breast, cervix, endometrium, gall bladder, fallopian tube, heart muscle, kidney, liver, pancreas, parathyroid, prostate, rectum, retina, small intestine, stomach, testis, urinary bladder, thyroid, placenta, ovary. Each dot in the figure represents the value obtained from an individual participant. Data are presented as the mean. Significant p-values are described in the image, as determined by One-way ANOVA with Tukey multiple comparisons test.

Supplementary Figure 2. Comparisons of meninge and sciatic nerve stain with symptoms displayed by the Long COVID participants. A Mouse meninges stain divided by symptoms displayed by the participants, as brain fog, fatigue, dizziness, tinnitus, confusion, dysautonomia, and pain. **B** Mouse sciatic nerve stain divided by symptoms displayed by the participants, as brain fog, fatigue, dizziness, disorientation, confusion, dysautonomia, pain, memory, weakness, and headache. Each dot in the figure represents the value obtained from an individual participant. Data are presented as the mean. Significant p-values are described in the image, as determined by One-way ANOVA with Tukey multiple comparisons test.

Supplementary Figure 3. Long COVID participants have increased and diverse AAB against MED and USP family proteins. A. Size-exclusion chromatography (SEC) profiles of the purified proteins run in a Fast Protein Liquid Chromatography (FPLC). Purity was determined by peak integration with the ChromLab Software. **B**. ELISA and Area Uder Curve (AUC) analysis for top hit targets identified by Huprot. **C.** Volcano plot showing differential abandance (Log_2 Fold Change) of AAB targets identified by pulldown using hIgG from healthy controls and Long COVID participants with mouse brain homogenate followed by mass spec. **D**. Time course analysis of human IgG concentration by ELISA in brain homogenate and serum for four days post-injection. Each dot in the figure represents the value obtained from an individual mouse. Data are presented as the mean ±SD. Significant p values are described in the image, as determined by T-test for two groups comparison or one-way ANOVA corrected for multiple comparisons with Tukey test for multiple groups comparison.

Supplementary Figure 4. Symptoms evaluated in the passive transfer that were not associated with hot plate test and grip strength. Dose of 38 mg/kg of total IgG purified from healthy, convalescent controls and Long COVID participants were administered to 6-8 weeks-old C57BLl/6 female mice by intraperitoneal (IP) injection, which were followed up for 5 days. **A.** Hot plate test divided by symptoms displayed by the participants as fatigue, disorientation, tinnitus, memory, confusion, dizziness, brain fog, headache. **B** Grip strength test divided by participants that displayed fatigue, disorientation, memory, confusion, weakness, dizziness, brain fog, chronic pain and dysautonomia. Each dot in the figure represents the value obtained from an individual mouse. Each mouse received antibodies isolated from a single human participant.

Data are presented as the mean. Significant p values are described in the image, as determined by one-way ANOVA corrected for multiple comparisons with Tukey test.

Supplementary Figure 5. Symptoms evaluated in the passive transfer that were not associated with rotarod. Dose of 38 mg/kg of total IgG purified from healthy, convalescent controls and Long COVID participants were administered to 6-8 weeks-old C57BL/6 female mice by intraperitoneal (IP) injection, which were followed up for 5 days. **A.** Rotarod test divided by symptoms displayed by the participants as fatigue, disorientation, tinnitus, brain fog, confusion, weakness, memory, chronic pain, headache, and dysautonomia.

Supplementary Figure 6. Passive transfer does not induce anxiety like behavior, locomotion and cardiovascular function symptoms in mice. Dose of 38 mg/kg of total IgG purified from healthy, convalescent controls and Long COVID participants were administered to 6-8 weeks-old C57BL/6 female mice by intraperitoneal (IP) injection, which were followed up for 5 days. **A**. Cumulative time spent in the cente, cumulative time spent in the border and representative heat map showing mice movement in the open field test. **B**.Mean velocity, distance moved and time moving during the open field test. **C**. Cumulative time in open arms, cumulative time in closed arms and representative heatmap showing mice movement in the elevated zero maze test. **D**. Heart rate, mean blood pressure, systolic blood pressure and diastolic blood pressure measurements. Each dot in the figure represents the value obtained from an individual mouse. Each mouse received antibodies isolated from a single human participant. Data are presented as mean. Significant p values are described in the image, as determined by one-way ANOVA corrected for multiple comparisons with Tukey test.

References

1. Ford Nd Fau - Slaughter, D., Slaughter D Fau - Edwards, D., Edwards D Fau - Dalton, A., Dalton A Fau - Perrine, C., Perrine C Fau - Vahratian, A., Vahratian A Fau - Saydah, S., and Saydah, S. (2023). Long COVID and Significant Activity Limitation Among Adults, by Age - United States, June 1-13, 2022, to June 7-19, 2023. MMWR Morb Mortal Wkly Rep *72*, 866–870. 10.15585/mmwr.mm7232a3.
2. Hua, M.J., Gonakoti, S., Shariff, R., Corpuz, C., Acosta, R.A.H., Chang, H., Asemota, I., Gobbi, E., and Rezai, K. (2023). Prevalence and Characteristics of Long COVID 7-12 Months After Hospitalization Among Patients From an Urban Safety-Net Hospital: A Pilot Study. AJPM Focus *2*, 100091.
3. Ceban, F., Ling, S., Lui, L.M.W., Lee, Y., Gill, H., Teopiz, K.M., Rodrigues, N.B., Subramaniapillai, M., Di Vincenzo, J.D., Cao, B., et al. (2022). Fatigue and cognitive impairment in Post-COVID-19 Syndrome: A systematic review and meta-analysis. Brain Behav Immun *101*, 93-135.
4. Bowe, B., Xie, Y.A.-O., and Al-Aly, Z.A.-O. (2022). Acute and postacute sequelae associated with SARS-CoV-2 reinfection. Nat Med *28*, 2398-2405.
5. Ayoubkhani, D.A.-O., Bosworth, M.L., King, S., Pouwels, K.B., Glickman, M., Nafilyan, V.A.-O.X., Zaccardi, F., Khunti, K.A.-O., Alwan, N.A.-O., and Walker, A.S. (2022). Risk of Long COVID in People Infected With Severe Acute Respiratory Syndrome Coronavirus 2 After 2 Doses of a Coronavirus Disease 2019 Vaccine: Community-Based, Matched Cohort Study. Open Forum Infect Dis *9*, ofac464. 10.1093/ofid/ofac464.
6. Douaud, G.A.-O.X., Lee, S., Alfaro-Almagro, F., Arthofer, C.A.-O., Wang, C.A.-O., McCarthy, P., Lange, F.A.-O., Andersson, J.L.R., Griffanti, L., Duff, E., et al. (2022). SARS-CoV-2 is associated with changes in brain structure in UK Biobank. Nature *604*, 697-707. 10.1038/s41586-022-04569-5.
7. Graham, E.A.-O., Clark, J.A.-O., Orban, Z.S., Lim, P.H., Szymanski, A.L., Taylor, C., DiBiase, R.M., Jia, D.T., Balabanov, R., Ho, S.U., et al. (2021). Persistent neurologic symptoms and cognitive dysfunction in non-hospitalized Covid-19 "long haulers". Ann Clin Transl Neurol *8*, 1073-1085. 10.1002/acn3.51350.
8. Salari, N., Khodayari, Y., Hosseinian-Far, A., Zarei, H., Rasoulpoor, S., Akbari, H., and Mohammadi, M.A.-O. (2022). Global prevalence of chronic fatigue syndrome among long COVID-19 patients: A systematic review and meta-analysis. Biopsychosoc Med *16*, 21.
9. Jason, L.A.-O., and Dorri, J.A. (2023). ME/CFS and Post-Exertional Malaise among Patients with Long COVID. Neurol Int *15*, 1-11.
10. Lim, E.J., Ahn, Y.C., Jang, E.S., Lee, S.W., Lee, S.H., and Son, C.A.-O. (2020). Systematic review and meta-analysis of the prevalence of chronic fatigue syndrome/myalgic encephalomyelitis (CFS/ME). J Transl Med *18*, 100. 10.1186/s12967-020-02269-0.
11. Beyond Myalgic Encephalomyelitis/Chronic Fatigue Syndrome: Redefining an Illness. (2015). Mil Med *180*, 721-723. 10.7205/MILMED-D-15-00085.
12. Abu Hamdh, B., and Nazzal, Z.A.-O. (2023). A prospective cohort study assessing the relationship between long-COVID symptom incidence in COVID-19 patients and COVID-19 vaccination. Sci Rep *13*, 4896. 10.1038/s41598-023-30583-2.

13. Bai, F., Tomasoni, D., Falcinella, C., Barbanotti, D., Castoldi, R., Mulè, G., Augello, M., Mondatore, D., Allegrini, M., Cona, A., et al. (2022). Female gender is associated with long COVID syndrome: a prospective cohort study. Clin Microbiol Infect *28*, 611.e619-611.e616. 10.1016/j.cmi.2021.11.002.
14. Wang, E.Y., Mao, T., Klein, J., Dai, Y., Huck, J.D., Jaycox, J.R., Liu, F., Zhou, T., Israelow, B., Wong, P., et al. (2021). Diverse functional autoantibodies in patients with COVID-19. Nature *595*, 283-288. 10.1038/s41586-021-03631-y.
15. Mulder, J., Lindqvist, I., Rasmusson, A.J., Husén, E., Rönnelid, J., Kumlien, E., Rostami, E., Virhammar, J., and Cunningham, J.L. (2021). Indirect immunofluorescence for detecting anti-neuronal autoimmunity in CSF after COVID-19 - Possibilities and pitfalls. . Brain Behav Immun *94*, 473-474.
16. Franke, C., Boesl, F., Goereci, Y., Gerhard, A., Schweitzer, F., Schroeder, M., Foverskov-Rasmussen, H., Heine, J., Quitschau, A., Kandil, F.I., et al. (2023). Association of cerebrospinal fluid brain-binding autoantibodies with cognitive impairment in post-COVID-19 syndrome. Brain Behav Immun *109*, 139-143.
17. Franke, C., Ferse, C., Kreye, J., Reincke, S.M., Sanchez-Sendin, E., Rocco, A., Steinbrenner, M., Angermair, S., Treskatsch, S., Zickler, D., et al. (2021). High frequency of cerebrospinal fluid autoantibodies in COVID-19 patients with neurological symptoms. Brain, Behavior, and Immunity *93*, 415-419. https://doi.org/10.1016/j.bbi.2020.12.022.
18. McAlpine, L.S., Lifland, B., Check, J.R., Angarita, G.A., Ngo, T.T., Chen, P., Dandekar, R., Alvarenga, B.D., Browne, W.D., Pleasure, S.J., et al. (2023). Anti-SARS-CoV-2 and Autoantibody Profiling of a COVID-19 Patient With Subacute Psychosis Who Remitted After Treatment With Intravenous Immunoglobulin. Biol Psychiatry *93*, e25-e29.
19. Muri, J., Cecchinato, V., Cavalli, A., Shanbhag, A.A., Matkovic, M., Biggiogero, M., Maida, P.A., Moritz, J., Toscano, C., Ghovehoud, E., et al. (2023). Autoantibodies against chemokines post-SARS-CoV-2 infection correlate with disease course. Nature Immunology *24*, 604-611. 10.1038/s41590-023-01445-w.
20. Szewczykowski, C., Mardin, C., Lucio, M., Wallukat, G., Hoffmanns, J., Schröder, T., Raith, F., Rogge, L., Heltmann, F., Moritz, M., et al. (2022). Long COVID: Association of Functional Autoantibodies against G-Protein-Coupled Receptors with an Impaired Retinal Microcirculation. Int J Mol Sci *23*, 7209.
21. Wallukat, G., Hohberger, B., Wenzel, K., Fürst, J., Schulze-Rothe, S., Wallukat, A., Hönicke, A.S., and Müller, J. (2021). Functional autoantibodies against G-protein coupled receptors in patients with persistent Long-COVID-19 symptoms. J Transl Autoimmun *4*, 100100.
22. Woodruff, M.A.-O., Ramonell, R.P., Haddad, N.A.-O., Anam, F.A., Rudolph, M.A.-O., Walker, T.A., Truong, A.D., Dixit, A.N., Han, J.A.-O., Cabrera-Mora, M., et al. Dysregulated naive B cells and de novo autoreactivity in severe COVID-19.
23. Etter, M.M., Martins, T.A., Kulsvehagen, L., Pössnecker, E., Duchemin, W., Hogan, S., Sanabria-Diaz, G., Müller, J., Chiappini, A., Rychen, J., et al. (2022). Severe Neuro-COVID is associated with peripheral immune signatures, autoimmunity and neurodegeneration: a prospective cross-sectional study. Nature Communications *13*, 6777. 10.1038/s41467-022-34068-0.
24. Freitag, H.A.-O., Szklarski, M.A.-O., Lorenz, S., Sotzny, F., Bauer, S., Philippe, A., Kedor, C., Grabowski, P., Lange, T.A.-O., Riemekasten, G., et al. (2021). Autoantibodies to Vasoregulative G-Protein-Coupled Receptors Correlate with Symptom Severity,

Autonomic Dysfunction and Disability in Myalgic Encephalomyelitis/Chronic Fatigue Syndrome. J Clin Med *10*, 3675. 10.3390/jcm10163675.

25. Ryabkova, V.A.-O., Gavrilova, N.Y., Poletaeva, A.A., Pukhalenko, A.I., Koshkina, I.A., Churilov, L.A.-O., and Shoenfeld, Y. (2023). Autoantibody Correlation Signatures in Fibromyalgia and Myalgic Encephalomyelitis/Chronic Fatigue Syndrome: Association with Symptom Severity. Biomedicines *11*, 257. 10.3390/biomedicines11020257.
26. Loebel, M., Grabowski, P., Heidecke, H., Bauer, S., Hanitsch, L.G., Wittke, K., Meisel, C., Reinke, P., Volk, H.D., Fluge, Ø., et al. (2016). Antibodies to β adrenergic and muscarinic cholinergic receptors in patients with Chronic Fatigue Syndrome. Brain Behav Immun *52*, 32-39. 10.1016/j.bbi.2015.09.013.
27. Chandra, A., Wormser Gp Fau - Klempner, M.S., Klempner Ms Fau - Trevino, R.P., Trevino Rp Fau - Crow, M.K., Crow Mk Fau - Latov, N., Latov N Fau - Alaedini, A., and Alaedini, A. (2010). Anti-neural antibody reactivity in patients with a history of Lyme borreliosis and persistent symptoms. Brain Behav Immun *24*, 1018-1024. 10.1016/j.bbi.2010.03.002.
28. Sloupenska, K.A.-O., Koubkova, B., Horak, P.A.-O.X., Hutyrova, B., Racansky, M., Mares, J., Miklusova, M., Schovanek, J., Zapletalova, J., Raska, M.A.-O., and Krupka, M.A.-O. (2023). Myositis Autoantibodies in Patients with Suspected Post-Treatment Lyme Disease Syndrome. Life (Basel) *13*, 527.
29. Gauntt, C.J., Arizpe Hm Fau - Higdon, A.L., Higdon Al Fau - Wood, H.J., Wood Hj Fau - Bowers, D.F., Bowers Df Fau - Rozek, M.M., Rozek Mm Fau - Crawley, R., and Crawley, R. (1995). Molecular mimicry, anti-coxsackievirus B3 neutralizing monoclonal antibodies, and myocarditis. J Immunol *154*, 2983-2995.
30. Lanz, T.A.-O., Brewer, R.A.-O., Ho, P.A.-O.X., Moon, J.A.-O.X., Jude, K.A.-O., Fernandez, D.A.-O.X., Fernandes, R.A., Gomez, A.M., Nadj, G.S., Bartley, C.A.-O., et al. (2022). Clonally expanded B cells in multiple sclerosis bind EBV EBNA1 and GlialCAM. Nature *603*, 321-327.
31. Leis, A.A., Szatmary G Fau - Ross, M.A., Ross Ma Fau - Stokic, D.S., and Stokic, D.S. (2014). West nile virus infection and myasthenia gravis. Muscle Nerve *49*, 26-29.
32. Vasilevska, V., Guest, P.C., Bernstein, H.G., Schroeter, M.L., Geis, C., and Steiner, J.A.-O. (2021). Molecular mimicry of NMDA receptors may contribute to neuropsychiatric symptoms in severe COVID-19 cases. J Neuroinflammation *18*, 245.
33. Zhao, Z.S., Granucci F Fau - Yeh, L., Yeh L Fau - Schaffer, P.A., Schaffer Pa Fau - Cantor, H., and Cantor, H. (1998). Molecular mimicry by herpes simplex virus-type 1: autoimmune disease after viral infection. Science *279*, 1344-1347.
34. Neumann, D.A., Rose Nr Fau - Ansari, A.A., Ansari Aa Fau - Herskowitz, A., and Herskowitz, A. (1994). Induction of multiple heart autoantibodies in mice with coxsackievirus B3- and cardiac myosin-induced autoimmune myocarditis. J Immunol *152*, 343-350.
35. Song, E., Bartley, C.M., Chow, R.D., Ngo, T.T., Jiang, R., Zamecnik, C.R., Dandekar, R., Loudermilk, R.P., Dai, Y., Liu, F., et al. (2021). Divergent and self-reactive immune responses in the CNS of COVID-19 patients with neurological symptoms. Cell Rep Med *2*, 100288.
36. Peng, K., Li, X., Yang, D., Chan, S.C.W., Zhou, J., Wan, E.Y.F., Chui, C.S.L., Lai, F.T.T., Wong, C.K.H., Chan, E.W.Y., et al. (2023). Risk of autoimmune diseases

following COVID-19 and the potential protective effect from vaccination: a population-based cohort study. EClinicalMedicine *63*, 102154.

37. Chang, R., Yen-Ting Chen, T., Wang, S.I., Hung, Y.M., Chen, H.Y., and Wei, C.J. (2023). Risk of autoimmune diseases in patients with COVID-19: A retrospective cohort study. EClinicalMedicine *56*, 101783. 10.1016/j.eclinm.2022.101783.
38. Tesch, F., Ehm, F., Vivirito, A., Wende, D., Batram, M., Loser, F., Menzer, S., Jacob, J., Roessler, M., Seifert, M., et al. (2023). Incident autoimmune diseases in association with SARS-CoV-2 infection: a matched cohort study. Clin Rheumatol *42*, 2905-2914. 10.1007/s10067-023-06670-0.
39. Syed, U., Subramanian, A., Wraith, D.C., Lord, J.M., McGee, K., Ghokale, K., Nirantharakumar, K., and Haroon, S. (2023). Incidence of immune-mediated inflammatory diseases following COVID-19: a matched cohort study in UK primary care. BMC Med *21*, 363. 10.1186/s12916-023-03049-5.
40. Klein, J.A.-O., Wood, J., Jaycox, J.R., Dhodapkar, R.A.-O., Lu, P.A.-O.X., Gehlhausen, J.R., Tabachnikova, A., Greene, K., Tabacof, L., Malik, A.A., et al. (2023). Distinguishing features of long COVID identified through immune profiling. Nature *623*, 139-148. 10.1038/s41586-023-06651-y.
41. Lucas, C.A.-O., Vogels, C.B.F., Yildirim, I., Rothman, J.A.-O., Lu, P.A.-O.X., Monteiro, V., Gehlhausen, J.R., Campbell, M., Silva, J.A.-O., Tabachnikova, A., et al. (2021). Impact of circulating SARS-CoV-2 variants on mRNA vaccine-induced immunity. Nature *600*, 523-529. 10.1038/s41586-021-04085-y.
42. Mehnert, M., Li, W., Wu, C., Salovska, B., and Liu, Y.A.-O. (2019). Combining Rapid Data Independent Acquisition and CRISPR Gene Deletion for Studying Potential Protein Functions: A Case of HMGN1. Proteomics *19*, e1800438.
43. Wu, C., Ba, Q., Lu, D., Li, W., Salovska, B., Hou, P., Mueller, T., Rosenberger, G., Gao, E., Di, Y., et al. (2021). Global and Site-Specific Effect of Phosphorylation on Protein Turnover. Dev Cell *56*, 111-124.e116.
44. Bruderer, R., Bernhardt, O.M., Gandhi, T., Xuan, Y., Sondermann, J., Schmidt, M., Gomez-Varela, D., and Reiter, L. (2017). Optimization of Experimental Parameters in Data-Independent Mass Spectrometry Significantly Increases Depth and Reproducibility of Results. Mol Cell Proteomics *16*, 2296-2309.
45. Facer, P., Punjabi Pp Fau - Abrari, A., Abrari A Fau - Kaba, R.A., Kaba Ra Fau - Severs, N.J., Severs Nj Fau - Chambers, J., Chambers J Fau - Kooner, J.S., Kooner Js Fau - Anand, P., and Anand, P. (2011). Localisation of SCN10A gene product Na(v)1.8 and novel pain-related ion channels in human heart. Int Heart J *52*, 146-152.
46. Hovaguimian, A., and Gibbons, C.H. (2011). Diagnosis and treatment of pain in small-fiber neuropathy. Curr Pain Headache Rep *15*, 193-200.
47. Khennouf, L., Gesslein, B., Brazhe, A., Octeau, J.C., Kutuzov, N., Khakh, B.S., and Lauritzen, M. (2018). Active role of capillary pericytes during stimulation-induced activity and spreading depolarization. Brain *141*, 2032-2046.
48. Savastano, M., Bottin R Fau - Andreoli, C., Andreoli C Fau - Marcon, M., and Marcon, M. (1995). Tinnitus as a Presenting Symptom in Secondary Neuropathy: a Case Report. Int Tinnitus J *1*, 153-154.
49. Chandan, H.S., Prabhu, P., and Deepthi, M. (2013). Prevalence and characteristics of tinnitus in individuals with auditory neuropathy spectrum disorder. Hearing, Balance and Communication *11*, 214-217. 10.3109/21695717.2013.821755.

50. Vasilkov, V., Caswell-Midwinter, B., Zhao, Y., de Gruttola, V., Jung, D.H., Liberman, M.C., and Maison, S.F. (2023). Evidence of cochlear neural degeneration in normal-hearing subjects with tinnitus. Sci Rep *13*, 19870. 10.1038/s41598-023-46741-5.
51. Merad, M.A.-O., Blish, C.A.-O., Sallusto, F.A.-O., and Iwasaki, A.A.-O. (2022). The immunology and immunopathology of COVID-19. *375*, 1122-1127.
52. Vodopiutz, J., Schmook Mt Fau - Konstantopoulou, V., Konstantopoulou V Fau - Plecko, B., Plecko B Fau - Greber-Platzer, S., Greber-Platzer S Fau - Creus, M., Creus M Fau - Seidl, R., Seidl R Fau - Janecke, A.R., and Janecke, A.R. (2015). MED20 mutation associated with infantile basal ganglia degeneration and brain atrophy. Eur J Pediatr *174*, 113-118.
53. Schiano, C., Luongo, L., Maione, S., and Napoli, C. (2023). Mediator complex in neurological disease. Life Sci *329*, 121986.
54. García-Caballero, A., Gadotti, V.M., Stemkowski, P., Weiss, N., Souza, I.A., Hodgkinson, V., Bladen, C., Chen, L., Hamid, J., Pizzoccaro, A., et al. (2014). The deubiquitinating enzyme USP5 modulates neuropathic and inflammatory pain by enhancing Cav3.2 channel activity. Neuron *83*, 1144-1158.
55. Nimmerjahn, F., and Ravetch, J.V. (2008). Anti-inflammatory actions of intravenous immunoglobulin. Annu Rev Immunol *26*, 513-533.
56. Manganotti, P., Garascia, G., Furlanis, G., and Buoite Stella, A. (2023). Efficacy of intravenous immunoglobulin (IVIg) on COVID-19-related neurological disorders over the last 2 years: an up-to-date narrative review. Front Neurosci. *17*, 1159929.
57. McAlpine, L.A.-O., Zubair, A.A.-O., Joseph, P.A.-O., and Spudich, S. (2024). Case-Control Study of Individuals With Small Fiber Neuropathy After COVID-19. Neurol Neuroimmunol Neuroinflamm *11*, e200244.

Fig.1. Sá et al.

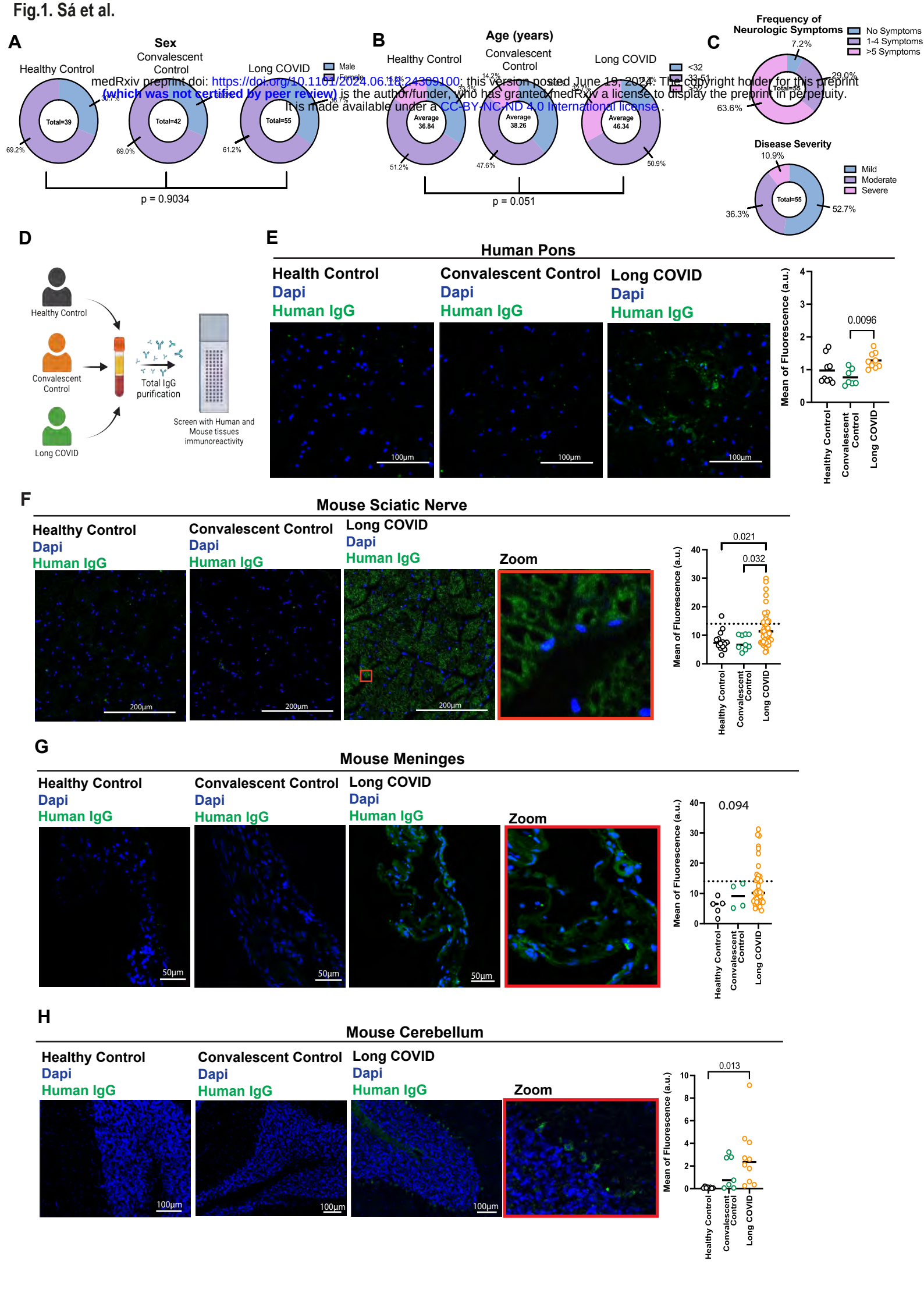

Fig.2. Sá et al.

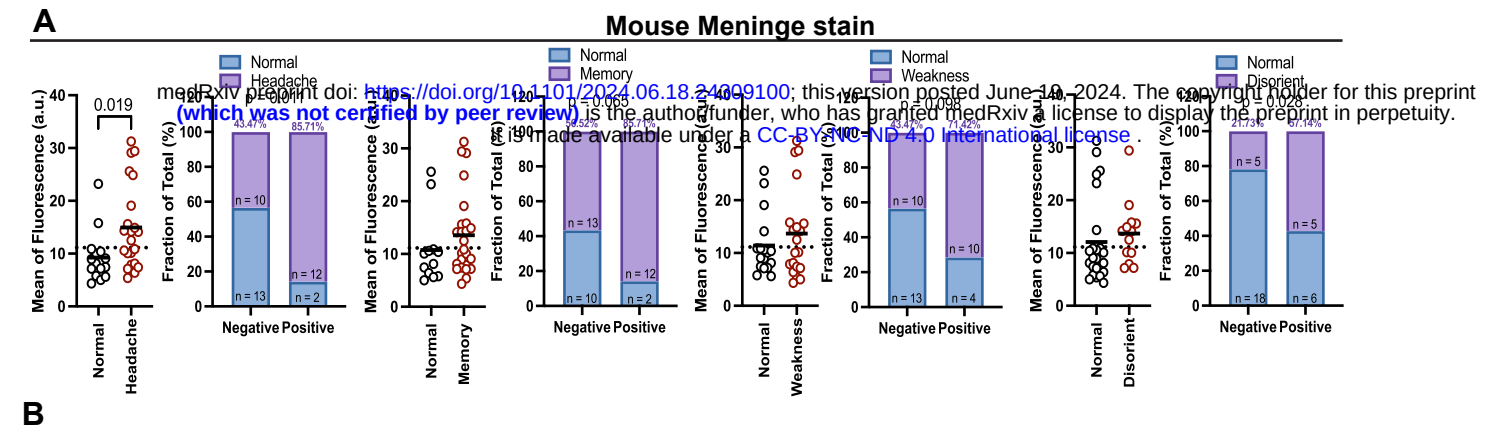

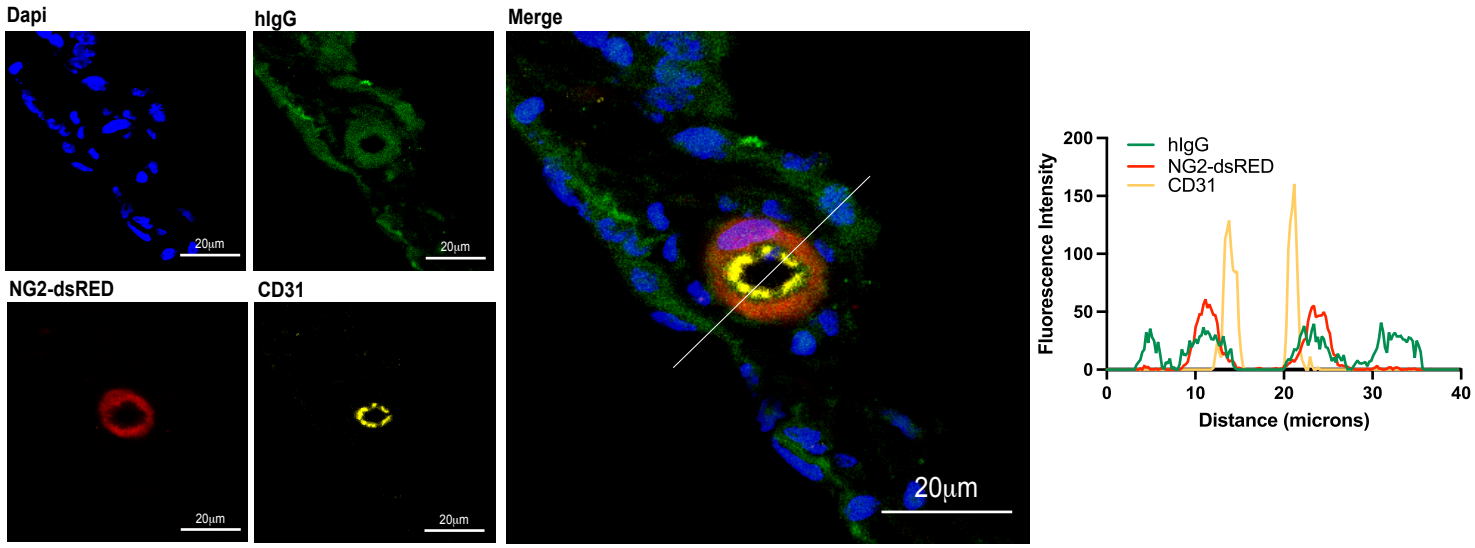

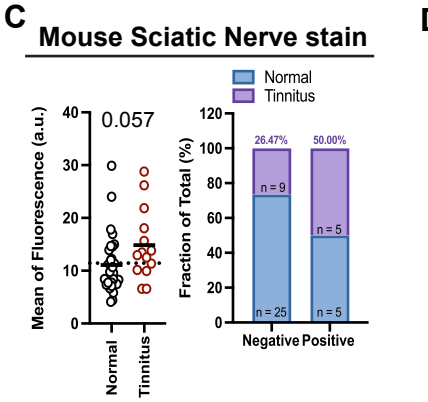

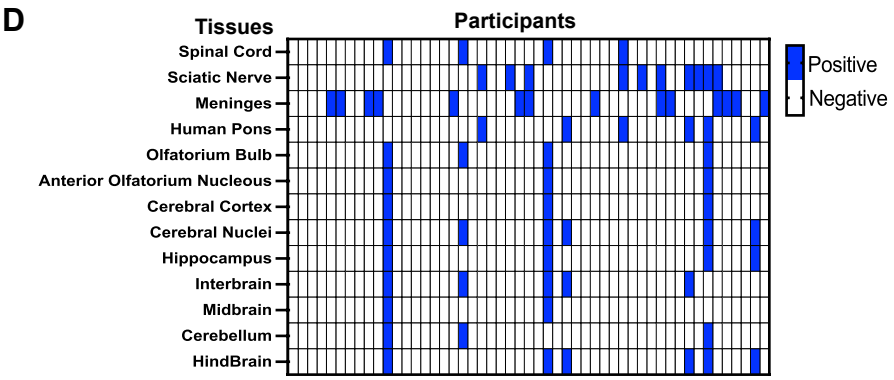

Fig.3. Sá et al.

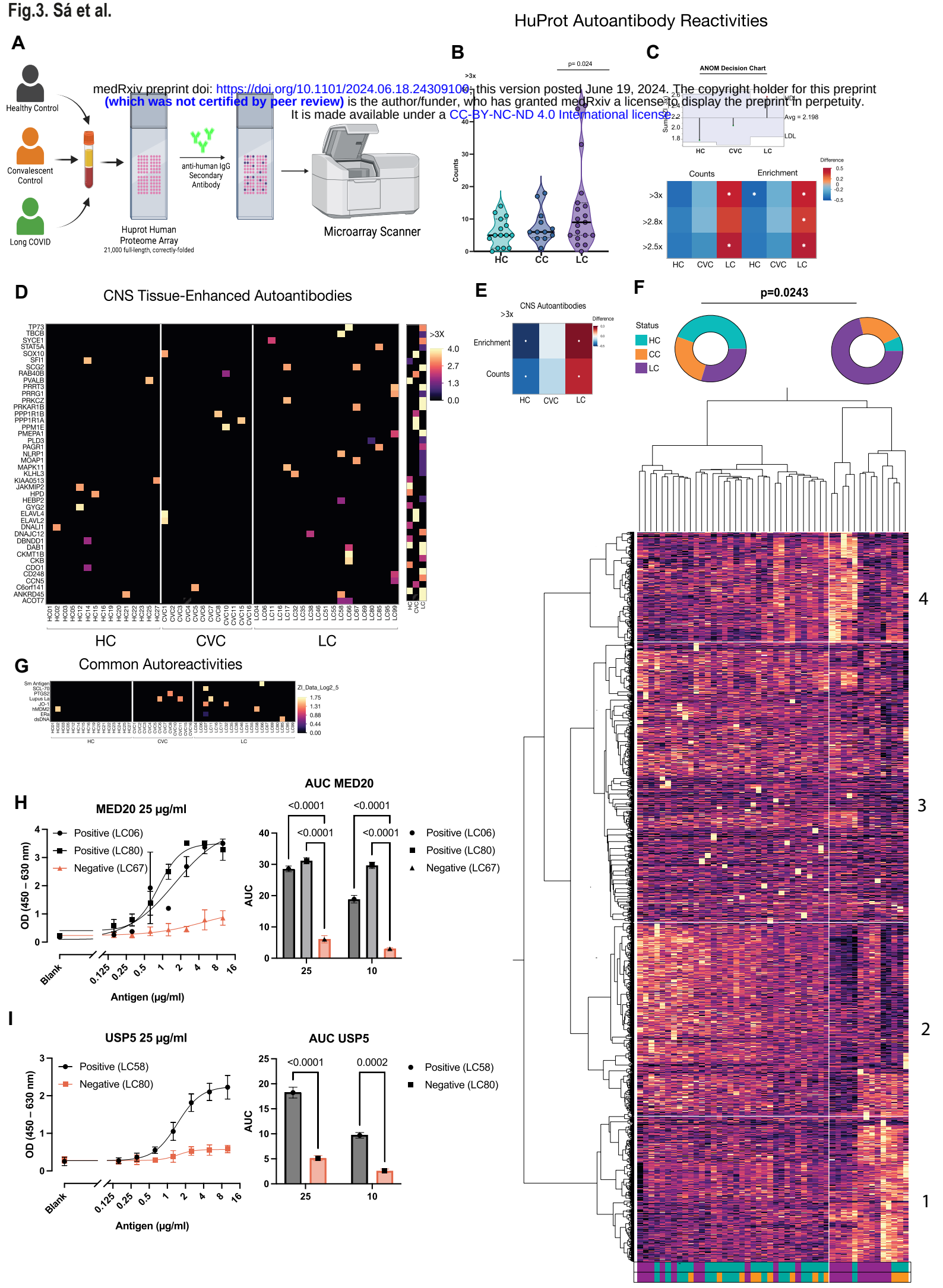

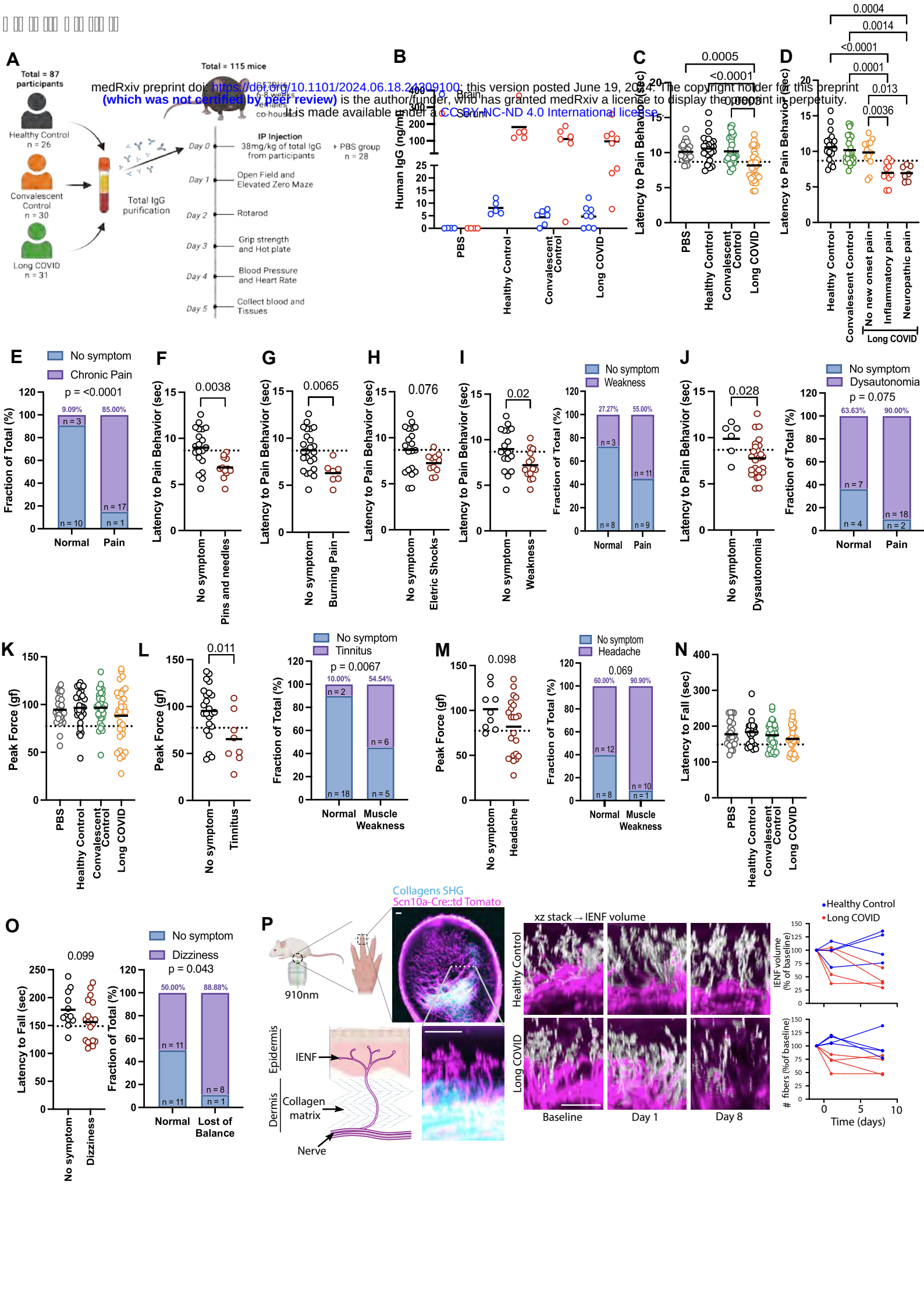

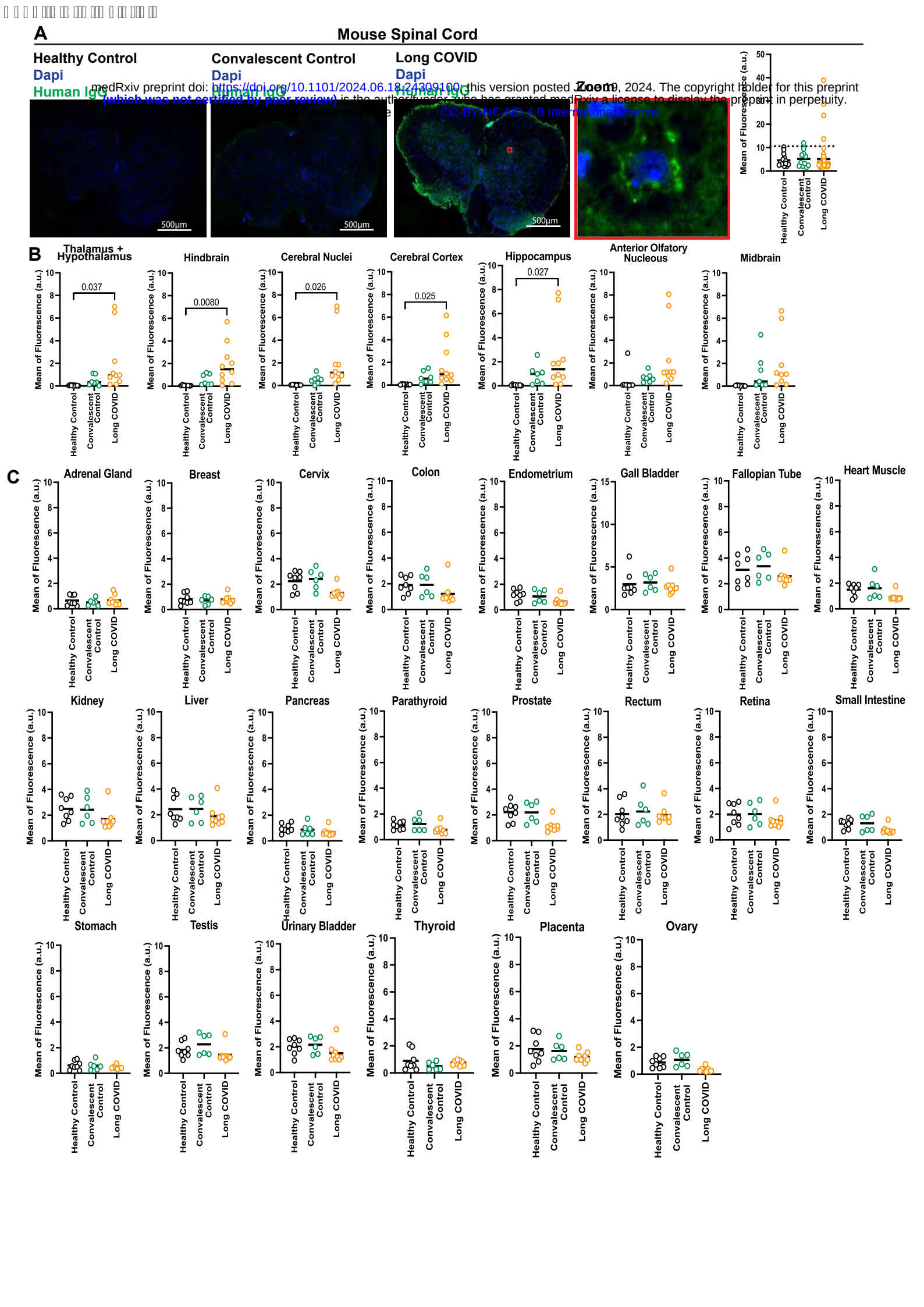

Supp. Fig. 2. Sá et al.

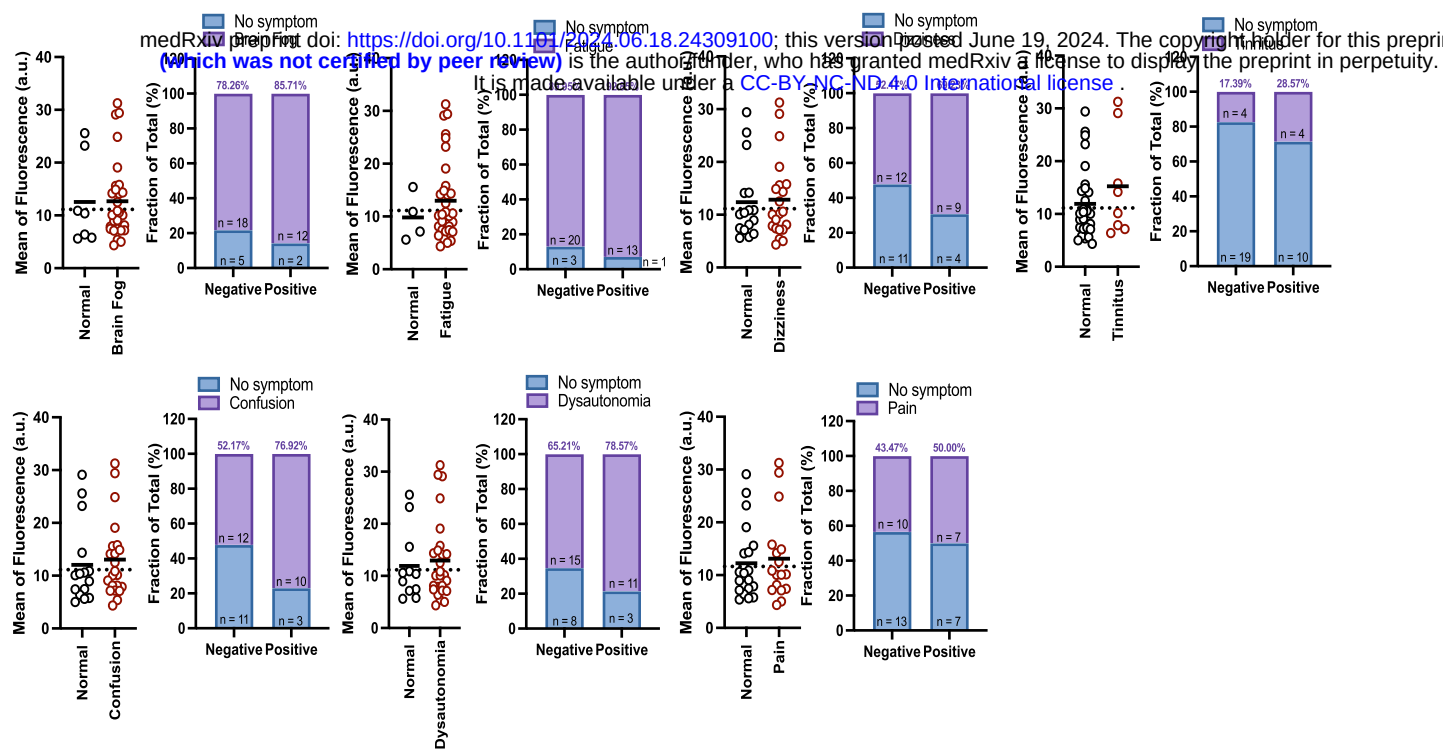

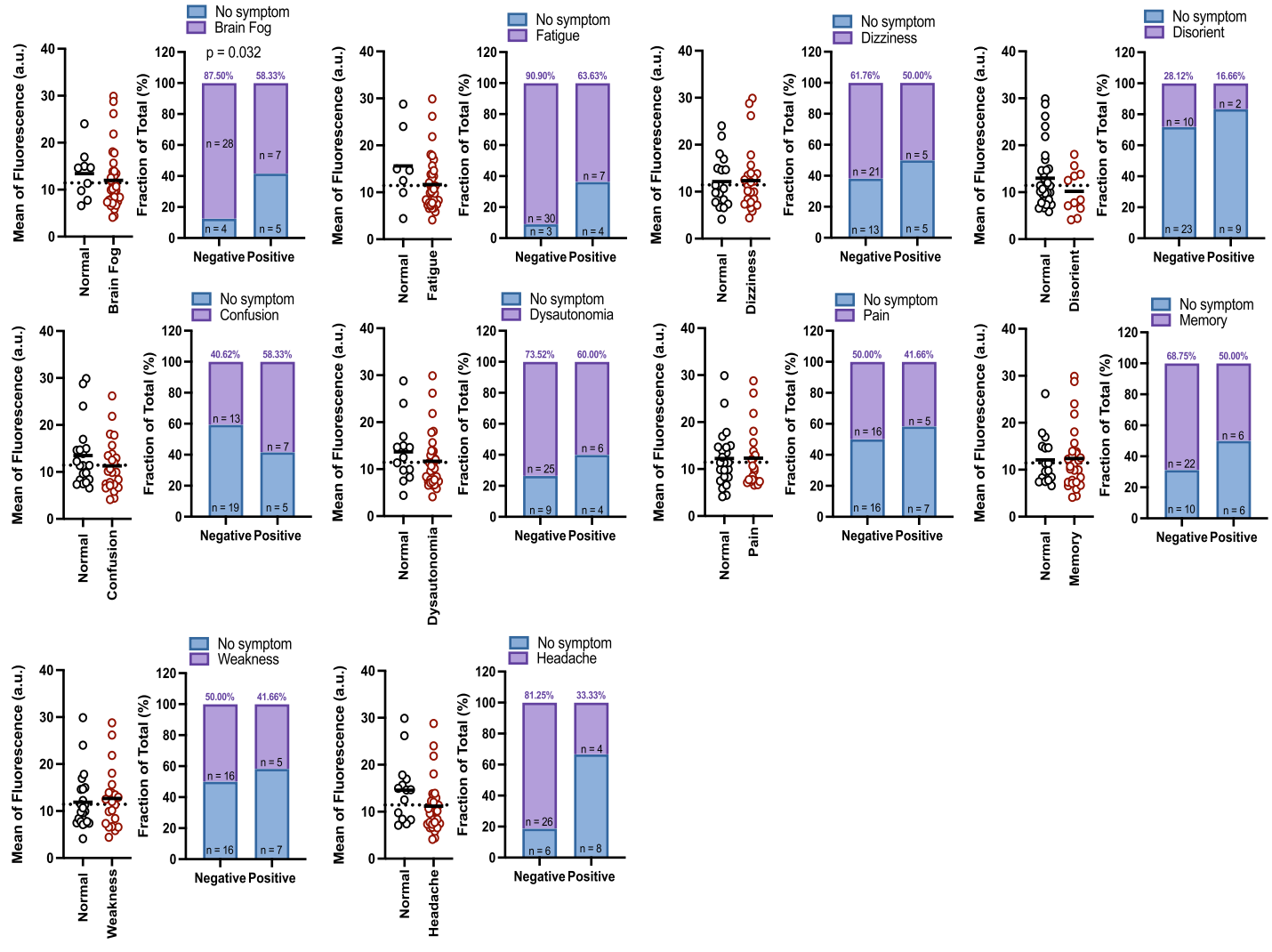

Supp. Fig. 3. Sá et al.

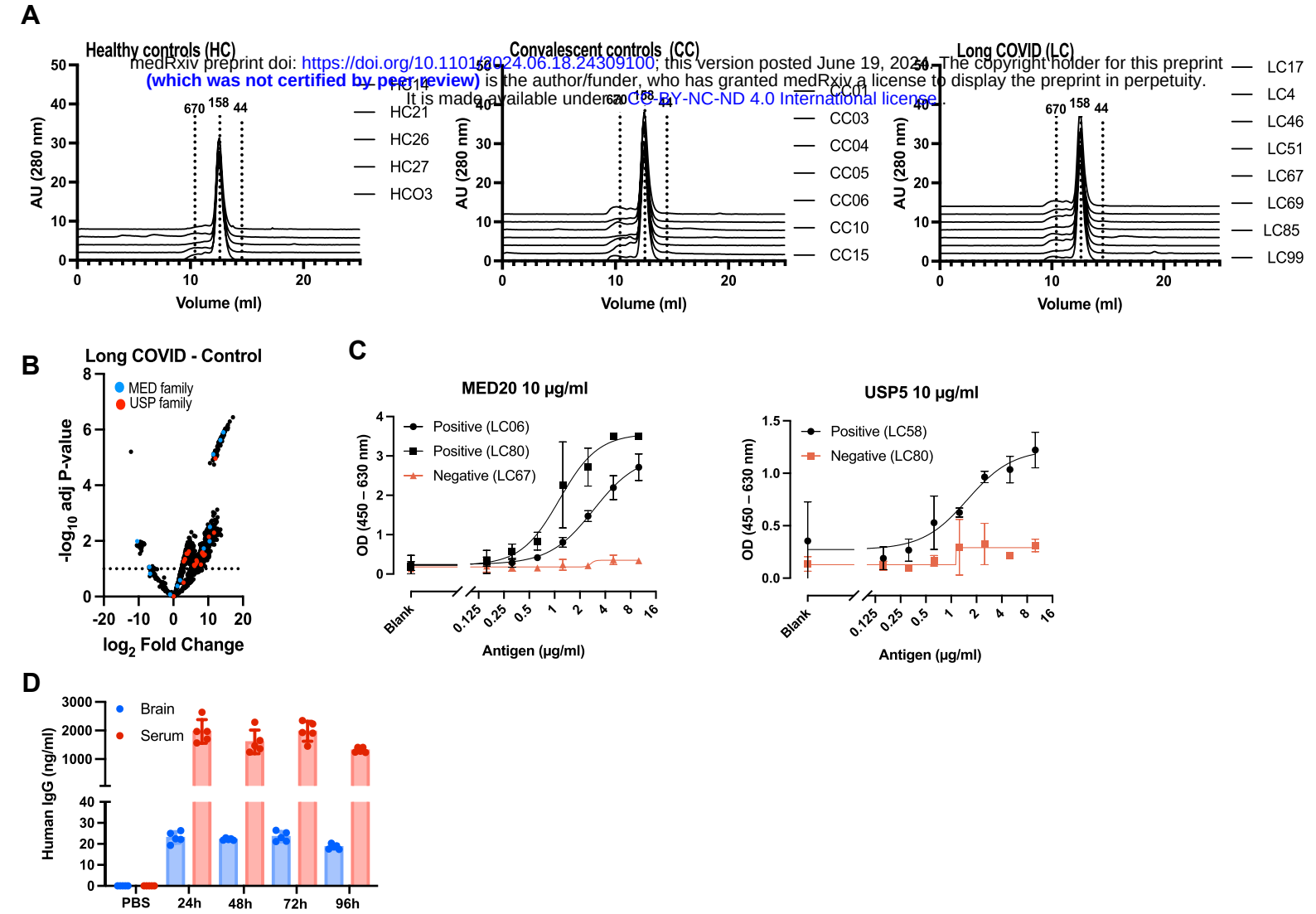

Supp. Fig. 4. Sá et al.

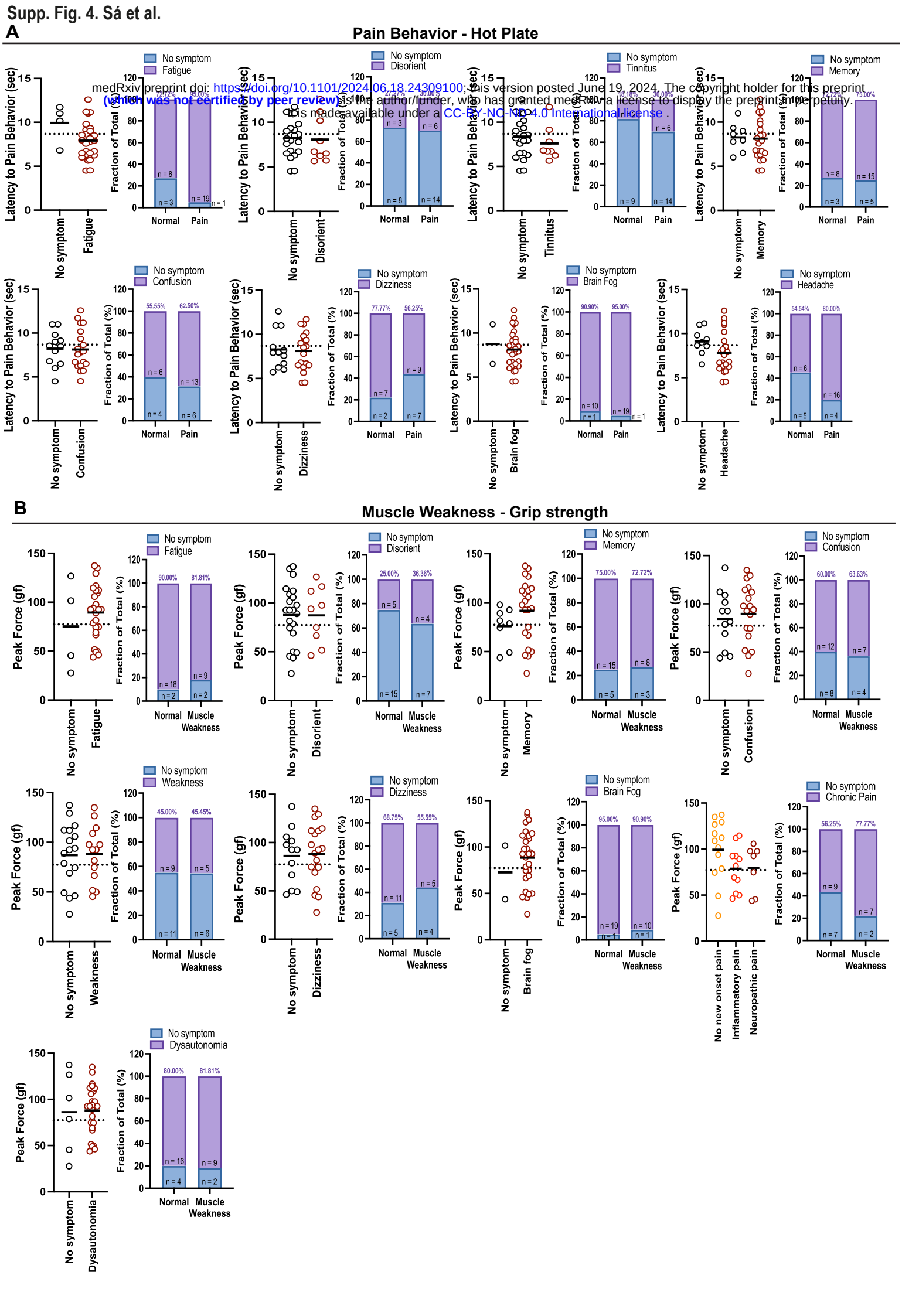

Supp. Fig. 5. Sá et al.

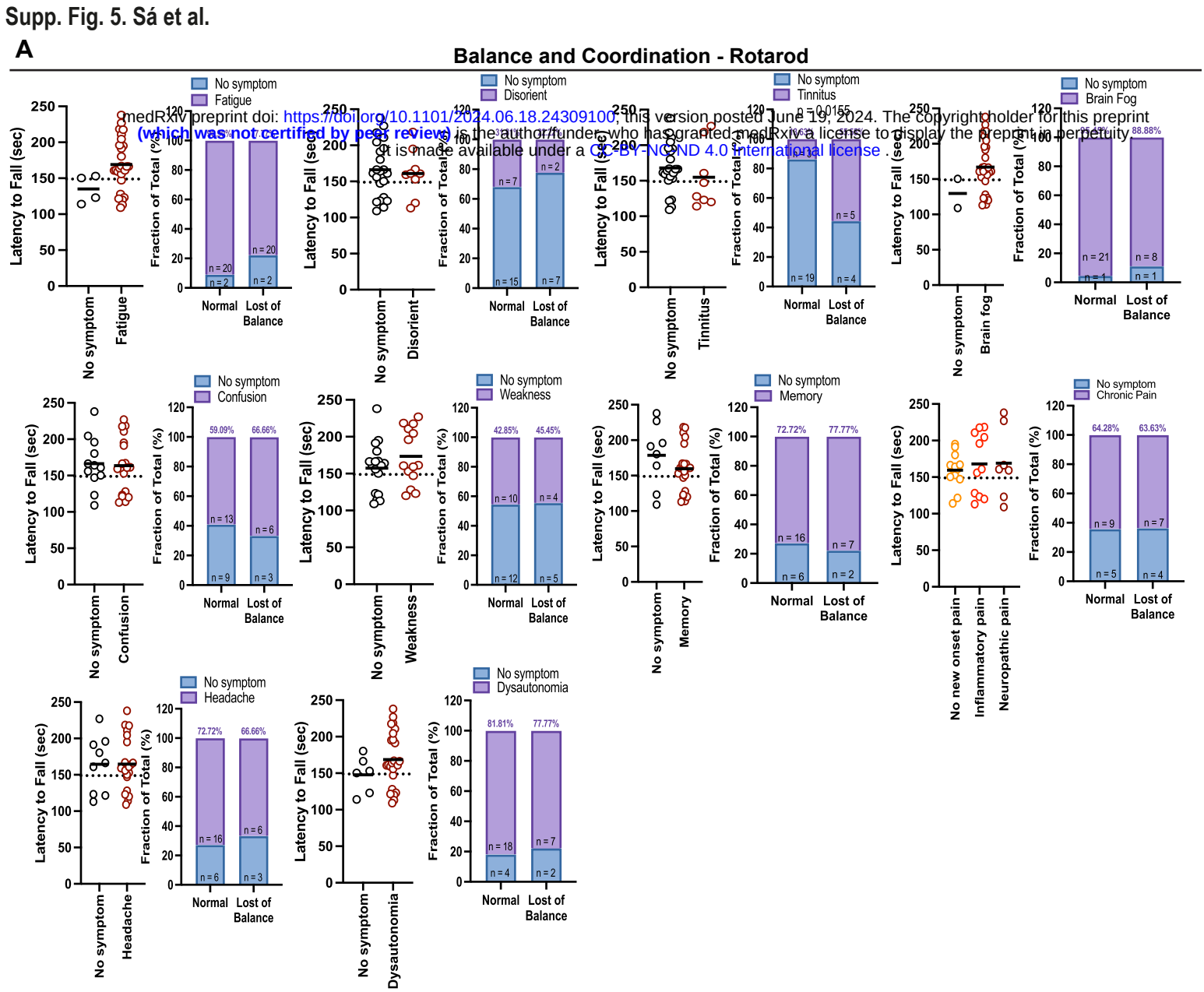

Supp. Fig. 6. Sá et al.